Korean J. Chem. Eng., **17**(2), 129-142 (2000)
FEATURED REVIEW

Computer Simulation of Diffusion within and through Membranes using Nonequilibrium Molecular Dynamics

J. M. Don MacElroy

Department of Chemical Engineering, Conway Institute of Biomolecular and Biomedical Research, University College Dublin, Belfield, Dublin 4, Ireland

Abstract−A novel nonequilibrium molecular dynamics (NEMD) method introduced in 1994 and its recent application to investigations of the transport properties of gases and dense fluids within strongly inhomogeneous pore structures are reviewed. In this technique molecular simulations are conducted under realistic nonequilibrium (experimental) conditions thus enabling direct insight into the underlying microscopic processes taking place during transport within pores. The case studies reviewed in this paper establish the versatility and scope of the NEMD technique and also demonstrate its significant advantages over prior molecular simulation procedures as a tool to assist in the design and tailoring of novel nanopore systems.

Key words: Diffusion, Membranes, Molecular Dynamics, Simulation

INTRODUCTION

The last decade has seen a significant growth in the development and implementation of novel strategies for nanostructure design and processing in a variety of advanced technological areas. These include the tailoring of new porous materials for highly selective separations and reactions, drug design in the pharmaceutical industry and fabrication of semiconductor composites in microelectronics. In parallel with experimental studies and engineering design of such systems, one particular methodology which has attracted the attention of many scientists and engineers and which is fast becoming an invaluable tool involves direct atomistic simulation of the microscopic phenomena taking place within these systems. Within the field of chemical engineering one particular area which is benefiting from computational work of this kind is the modelling of adsorption and transport of pure fluids and mixtures in microporous media and polymeric membranes and it is a specific topic in this general area, namely molecular simulation of diffusion through thin membranes, which is the subject of this paper.

1. Background

The molecular simulation method most frequently employed in the literature to predict species diffusion coefficients within porous media involves the computation of particle trajectories under *equilibrium* conditions (equilibrium molecular dynamics, EMD). This trajectory information is then coupled with general results provided by linear response theory [see Allen and Tildesley, 1987 for details] to provide estimates of the transport parameters. For example, in the absence of a net convective contribution to the fluxes and assuming isothermal conditions, the flux equation for component i in a multicomponent mixture within an isotropic homogeneous porous medium may be written as [Mason and Viehland, 1978; Mason and Malinauskas, 1983]

$$\mathbf{J}_i = -\sum_{i=1}^{\nu} \frac{D_{ij} n_i}{k_B T} \nabla_T \mu_i \tag{1}$$

The phenomenological diffusion coefficients D_{ij} are directly related to the d-dimensional time-correlation functions of the particle centre-of-mass velocities, $\mathbf{v}_\gamma(t)$ (Green-Kubo [Green 1952, 1954; Kubo et al., 1985]) or the centre of mass relative displacements, $\mathbf{r}_\gamma(t)-\mathbf{r}_\gamma(0)$ (after Einstein [see Berne, 1971]) by

$$D_{ij} = \frac{1}{dN_j} \int_0^\infty \langle \sum_{\alpha=1}^{N_i} \mathbf{v}_\alpha(t) . \sum_{\beta=1}^{N_j} \mathbf{v}_\beta(0) \rangle dt \tag{2a}$$

$$= \frac{1}{2dN_j} \lim_{t\to\infty} \frac{d}{dt} \langle \sum_{\alpha=1}^{N_i} (\mathbf{r}_\alpha(t)-\mathbf{r}_\alpha(0)) . \sum_{\beta=1}^{N_j} (\mathbf{r}_\beta(t)-\mathbf{r}_\beta(0)) \rangle \tag{2b}$$

n_i and μ_i are the local concentration and chemical potential of component i, T is the absolute temperature and N_i is the number of particles of component i within a macroscopically small though microscopically large (local equilibrium) volume element of the medium. The angular brackets in Eq. (2) represent averaging over an equilibrium ensemble of particles confined within the porous medium.

The application of computer simulation to the evaluation of the equilibrium time-correlation functions of confined fluids and mixtures is comparatively straightforward (details for simple model systems are provided in MacElroy, 1997), however this approach suffers serious difficulties when it is employed to compute (i) diffusivities within strongly inhomogeneous systems (e.g. ultrathin membranes) and (ii) diffusion within random media composed of both percolating and nonpercolating clusters.

For locally inhomogeneous systems nonlocal effects should, in general, be taken into consideration if equilibrium time-correlation function methods (via EMD) are to be used. This is most clearly demonstrated, for example, in the case of multicomponent bulk fluid mixtures by the more general results for the microscopic (isothermal) diffusion flux of component i reported by Mori [1965] [see also Altenberger et al., 1987] which, in frequency and wave vector space, is succinctly expressed as

†To whom correspondence should be addressed.
E-mail: Don.MacElroy@ucd.ie

$$\mathbf{j}_i(\mathbf{k},\omega)=\mathbf{j}_i^r(\mathbf{k},\omega)-\sum_{j=1}^{\nu}L_{ij}^r(\mathbf{k},\omega)i\mathbf{k}\delta_T\mu_j(\mathbf{k},\omega) \quad (3)$$

where $\mathbf{j}_i^r(\mathbf{k},\omega)$ is the 'random' component of the microscopic current of particles of component i which is orthogonal to the space spanned by the density fluctuations and the second term corresponds to the systematic component arising directly from density fluctuations. $L_{ij}^r(\mathbf{k},\omega)$ is an 'after-effect' coefficient for diffusion which is given by

$$L_{ij}^r(\mathbf{k},\omega)=\frac{1}{k^2k_BT}\mathbf{k}.\langle\mathbf{j}_i^r(\mathbf{k},\omega)\mathbf{j}_i^r(-\mathbf{k},0)\rangle.\mathbf{k} \quad (4)$$

and which is related to the more familiar linear response coefficients through the expression [Altenberger et al., 1987]

$$\mathbf{L}^r(\mathbf{k},\omega)=\mathbf{L}(\mathbf{k},\omega)[\mathbf{1}-\mathbf{F}(\mathbf{k},\omega)]^{-1} \quad (5)$$

The elements of the matrix **L** in this equation are

$$L_{ij}(\mathbf{k},\omega)=\frac{1}{k^2k_BT}\mathbf{k}.\langle\mathbf{j}_i(\mathbf{k},\omega)\mathbf{j}_i(-\mathbf{k},0)\rangle.\mathbf{k} \quad (6a)$$

and $\mathbf{F}(\mathbf{k},\omega)$ is a matrix with elements

$$F_{ij}(k)=(k_BT)^{-1}\langle\delta_T\mu_i(\mathbf{k},\omega)\imath\mathbf{k}.\mathbf{j}_j(-\mathbf{k},0)\rangle \quad (6b)$$

It is important to note that the microscopic currents appearing in the expression for the linear response coefficients $L_{ij}(\mathbf{k},\omega)$ correspond to the *mechanical* form

$$\mathbf{j}_i(\mathbf{k},t)=V^{-1/2}\sum_{l=1}^{N_i}\mathbf{v}_{li}(t)\exp(-i\mathbf{k}.\mathbf{r}_{li}) \quad (7)$$

and are not the random currents $\mathbf{j}_i^r(\mathbf{k},t)$ which are much more difficult to compute.

For comparatively small wave numbers and for low though nonzero frequencies $\mathbf{j}_i^r(\mathbf{k},\omega)\rightarrow\mathbf{0}$ and the isothermal (macroscopically observed) flux is

$$\mathbf{J}_i(\mathbf{r},t)=-\sum_{j=1}^{\nu}\int_0^t\int_v L_{ij}^r(\mathbf{r}-\mathbf{r}',t-\tau).\nabla_T\mu_j(\mathbf{r}',\tau)d\mathbf{r}'d\tau \quad (8)$$

where $L_{ij}^r(\mathbf{r},t)$ is the inverse Laplace-Fourier transform of Eq. (5).

If the spatial range of sampling, V, is sufficiently large on a microscopic scale to include all possible inhomogeneities then spatial nonlocality disappears and for an isotropic system we obtain the considerably simplified result

$$\mathbf{J}_i(\mathbf{r},t)=-\frac{1}{3Vk_BT}\sum_{j=1}^{\nu}\int_0^t C_{ij}(t-\tau)\nabla_T\mu_j(\mathbf{r},\tau)d\tau \quad (9)$$

where $C_{ij}(t)$ is the velocity time-correlation function

$$C_{ij}(t)=\langle\sum_{l=1}^{N_i}\mathbf{v}_{li}(t).\sum_{k=1}^{N_j}\mathbf{v}_{kj}(0)\rangle$$

Eq. (9) further simplifies to Eq. (1) in the stationary limit ($t\rightarrow\infty$) with the diffusion coefficients D_{ij} given by Eq. (2).

The spatial (nonzero **k**) and temporal (nonzero ω) nonlocal contributions in the general theory arise due to the distinct variations in the environment in which a diffusing particle finds itself as its trajectory evolves. The range over which these nonlocal effects are observed in practice is typically of the order of a few tens of Å^3 and picoseconds for simple homogeneous fluids and these scales increase significantly for media with long-ranged inhomogeneities (membranes or composites) or heterogeneities (semicrystalline or amorphous materials) and/or which are subject to low frequency relaxation processes (polymers). To the author's knowledge the only studies reported in the literature which have attempted to account for nonlocal or spatial effects of this kind are the work of Vertenstein and Ronis, 1986, and more recently, Pozhar and Gubbins, 1993, 1997. Vertenstein and Ronis investigated single particle (tracer) diffusion at the pore mouth and within a model protein channel of finite length and their analysis clearly demonstrates that the evaluation of the nonlocal terms significantly complicates the EMD computational procedure. The theoretical results of Pozhar and Gubbins have yet to be applied to quantify diffusion in confined fluids however this theory does look very promising and should prove essential in future studies of transport in nanopores.

The second area (which is not unrelated to the above in many respects) in which EMD techniques encounter obstacles is in the computation of diffusion within semi-percolating systems. In practical applications of sorption and diffusion within porous media and membranes a sorbate-free porous solid is usually exposed to the sorbate mixture with subsequent separation (and/or reaction) of the mixture taking place as a result of diffusion along percolating pathways to the sorption (reaction) sites within the medium. In EMD simulations, the usual procedure involved in the computation of the time-correlation functions for diffusion in a random medium entails the creation of static realisations of the particles of the solid phase with subsequent random insertion of the fluid particles within the voids of the medium. By running a conventional MD trajectory computation for all of the particles inserted in this manner it is quite possible that a significant number of the particles are actually trapped (depending on the relative proximity to the percolation threshold for the given solid/fluid pair) and should not be included in the evaluation of the true diffusivity

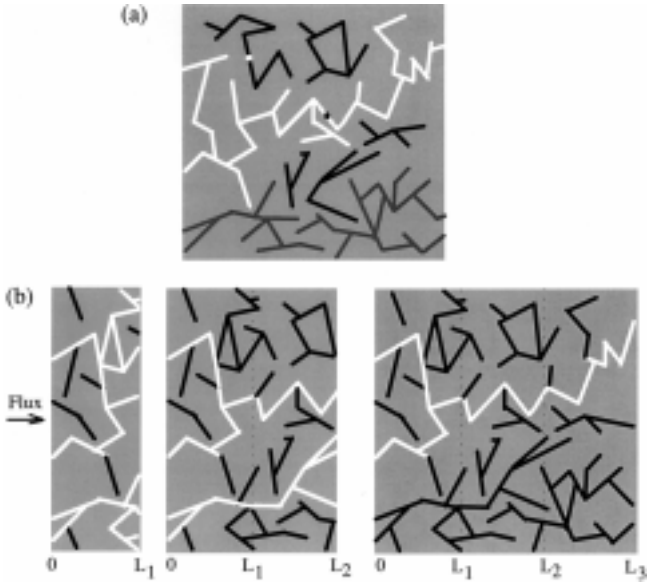

Fig. 1. Model pore structures. (a) An homogeneous medium with sample spanning (percolating) pores in white, dead end pores in grey and closed pores in black. (b) An inhomogeneous medium of three thicknesses. With reference to the direction of particle flow the sample spanning pores are in white and nonpercolating pores are in black.

within the medium. This problem is illustrated schematically in Fig. 1(a) for an 'infinite' medium. The white pore structure is accessible from both left and right (i.e. sample spanning) while the dark grey pores are only accessible from either the left or the right. Both of these regions of the pore space would be deemed open to the surroundings in an uptake experiment of the kind described above. The small black circle then represents a permissible location to place a particle. The black pores on the other hand are inaccessible and the white particle placed as shown does not represent a valid insertion. While it is possible to overcome some of the difficulties associated with this problem using scaling theories for diffusion in mixed percolating/non-percolating clusters [Gefen et al., 1983] the explicit problem with the application of the EMD technique still remains.

A further situation which combines both the effects of finite spatial range and semi- or non-percolating conditions is illustrated in Fig. 1(b). Consider the situation in which a fluid mixture is diffusing from left to right. In the first diagram on the left of Fig. 1(b) the white pores are percolating pathways while the black pores represent either non-percolating paths or dead-end pores. In the second diagram the thickness of the medium is increased by a factor of two while retaining its general topological structure at a local level. In this case the number of spanning pathways is reduced and the flux of material consequently drops. A further increase in the thickness leads to the elimination of more percolating pathways with a further drop in flux. Taken to the limit, the porous medium may prove to be impermeable or semipermeable depending largely on how one specifies the *local* pore topology (except for an infinite medium located precisely at its percolation threshold in which case the pore topological characteristics of the system as a whole must be considered). As will be demonstrated later, diffusion in such systems cannot be investigated unambiguously using the EMD technique without additional information concerning the relative influence of the boundaries of the medium.

The desire to circumvent the difficulties outlined above formed the basis for the development of the novel molecular simulation method proposed by MacElroy, 1994, and Heffelfinger and van Swol, 1994, and it is this dual-control volume nonequilibrium molecular dynamics (NEMD) technique which is the focus of this paper. In Section 2 details of the NEMD technique as described by MacElroy, 1994, and Heffelfinger and van Swol, 1994, and in similar studies reported by Cracknell et al. [1995], Furukawa et al., 1996, and Xu et al., 1998, will be outlined and in Section 3 four case studies undertaken in this laboratory will be reviewed. The paper will close in Section 4 with a brief overview of related work and future directions.

NONEQUILIBRIUM MOLECULAR DYNAMICS SIMULATION OF DIFFUSION

The nonequilibrium simulation technique closely mimics real laboratory conditions for diffusivity or permeability measurements which have been used widely over the last four to five decades (see for example, Wicke and Kallenbach, 1941, for gases and Kaufman and Leonard, 1968, for liquids) and is best described with reference to Fig. 2. The fundamental cell for the molecular simulation

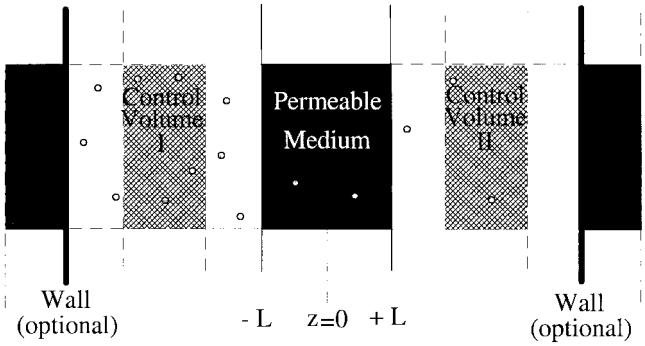

Fig. 2. The model system for nonequilibrium simulations. The central permeable region between –L<z<L is the region of interest were the nonequilibrium flows take place. The two control volumes on either side are maintained at specified thermodynamic states during the course of the simulations.

consists of two control volumes (regions I and II) on either side of the intermediate permeable (or semi-permeable) region which is of interest in the study (while in the present context this region is a membrane of specified structure (inhomogeneous system), it may also be simply an extension of the homogeneous fluid regions in the control volumes I and II if bulk homogeneous transport properties are of principal concern). The cell is periodically imaged in both the x and y directions (for details of periodic imaging as a tool in the general area of molecular simulation the reader is referred to the text by Allen and Tildesley, 1987). Imaging in the z direction may also be considered and has been employed by a number of workers [Heffelfinger and van Swol, 1994; Cracknell et al., 1995; and Furukawa et al., 1996] while in other studies (those discussed later in Section 3) the background walls indicated in Fig. 2 have been incorporated into the simulations.

The membrane and the fluid species to be investigated are modelled by specifying appropriate interatomic and/or intermolecular and intramolecular potential energy functions which may take on a variety of forms. These include nonbonded interactions (i.e. London-van der Waals forces, polar interactions due to permanent dipoles, quadrupoles etc., and electrostatic interactions) and bonded (intramolecular) interactions (three body bond angle bending and four body torsion potentials as well as bond stretching). In view of the range of possible membrane materials and fluids which may be encountered in practice, the analysis can vary from one extreme of comparative simplicity (simple atomic fluids in crystalline membranes of a pure material) to very complex systems (e.g. ion transport across protein forming channels in lipid membranes). Therefore, in the interests of clarity we will confine the discourse below to systems composed of membranes and fluids which interact by one or other of the following two simple interaction potentials:

(i) Hard core interactions:

$$\phi_{ij}(r_{ij}) = \infty \quad (r_{ij} < \sigma_{ij})$$
$$= 0 \quad (r_{ij} > \sigma_{ij}) \tag{10a}$$

where σ_{ij} is the separation distance between the centres of particles i and j at contact.

(i) London-van der Waals interactions as modelled by the Len-

nard-Jones (12-6) potential

$$\phi_{ij}(r_{ij})=4\varepsilon_{ij}\left[\left(\frac{\sigma_{ij}}{r_{ij}}\right)^{12}-\left(\frac{\sigma_{ij}}{r_{ij}}\right)^{6}\right] \quad (10b)$$

The use of these potentials will permit a demonstration of the basic principles of the nonequilibrium method.

Once the membrane and the fluid species have been selected for study then, in general, the simulation algorithm proceeds in two stages as follows:

(a) Initialisation: The length or thickness (2 L) of the membrane is specified and the grand canonical ensemble Monte Carlo (GCMC) simulation method of Adams, 1974, 1975 (fixed μ, V and T) is applied independently to the two regions of the simulation box $z<0$ and $z>0$ respectively if the permeable medium is fully percolating or simply to the fluid regions outside the medium if it is suspected that inaccessible domains exist within the membrane. The fluid components in both regions differ only with respect to their chemical potentials (or fugacities $\hat{f}_i$) and a uniform temperature is maintained throughout the cell. At the end of this initialisation stage the cell volume in the region $z<0$ (fully percolating system) or $z<-L$ (semi-percolating membrane) will contain a particular number of atoms or molecules of both species and the cell volume in the region $z>0$ (or $z>L$) will contain a different number of particles of both species. In subsequent computations (see Realisation below) the chemical potentials of both species are maintained at the preselected levels only within the control volumes I and II.

(b) Realisation: The particle velocities are now assigned from the Maxwell-Boltzmann distribution and the particle trajectories, at fixed particle number, are computed by solving the equations of motion. Depending on the nature of the intermolecular potentials one may compute the trajectories algebraically (hard core interactions) or by using one of a number of reported finite difference techniques (soft potentials). For reasons which will become clearer later, a particular case of the latter will be discussed in some detail below. As the particle trajectories evolve the particle depletion or accumulation within control volumes I and II is counterbalanced by periodically freezing the state of the system and conducting a short sequence of GCMC destruction/creation events on the fluid mixtures within control volumes I and II. For a given component i the prescription for the particle destruction/creation sequence is

$$\text{Destruction: acceptance if } \frac{P_\beta}{P_\alpha}=\frac{N_i RT}{\hat{f}_i V}\exp\left(-\frac{\Delta\Phi_{\alpha\beta}}{k_B T}\right)>\xi \quad (11a)$$

$$\text{Creation: acceptance if } \frac{P_\beta}{P_\alpha}=\frac{\hat{f}_i V}{(N_i+1)RT}\exp\left(-\frac{\Delta\Phi_{\alpha\beta}}{k_B T}\right)>\xi \quad (11b)$$

where P_β/P_α is the relative probability of observing two states β and α differing in potential energy by $\Delta\Phi_{\alpha\beta}$ and particle number by 1, N_i is the number of particles of component i present in state α, and ξ is a random number uniformly distributed on {0,1}. The prescription for undertaking the destruction/creation events (i.e. the frequency and number of such events at any given time) depends on a number of factors the most important of which are the size of the control volumes, the density or concentrations of the species in these volumes and the anticipated flux of material to or from the control volumes. While a careful assessment of these conditions must be considered in order to ensure the chemical potentials remain constant on both sides of the membrane, a generally useful guideline is to conduct these destruction/creation events every time neighborhood lists [Verlet, 1967] are updated. The actual number of events required to keep the control volumes at the required chemical potentials may then be determined from a few short preproduction simulation runs. After each sequence of destruction/creation events all of the newly created particles within control volumes I and II are assigned velocities from the appropriate Maxwell-Boltzmann distribution function at the specified temperature (the velocities and coordinates of all other particles are still stored and remain untouched) and the forces on each particle are evaluated from their known coordinates.

One particular decision which needs to be made before tackling a simulation of this kind is to choose whether the lattice atoms which make up the material in the membrane are mobile or not. Quite clearly if the solid material is assumed to be stationary then a very significant savings in computer time may be achieved. While this can result in a loss of some measure of realism (in polymeric membranes above the glass transition temperature it is in fact necessary to include these motions in order to obtain reliable predictions of the permeation characteristics) for many inorganic membranes it is possible under certain conditions to assume that the membrane atoms are static [Ford and Glandt, 1995; Haberlandt and Karger, 1999]. The underlying high frequency vibrational motion of the solid atoms (which constitutes the thermal reservoir available to the fluid particles as they diffuse across the system) may then be included using one or other of the thermostatting procedures reported in the literature (see Allen and Tildesley, 1987, for details) for systems at equilibrium (applied in the present nonequilibrium case at a local level assuming local thermal equilibrium) or preferably by using the novel fluid particle/membrane atom thermal collision process described recently in MacElroy and Boyle, 1999. The latter procedure applies the local equilibrium concept in a unique way at a *point* rather than in a finite volume element and hence limits the influence of the thermostatting on the nonequilibrium molecular flux profiles within the micropores of the membrane. This is done in such a way that the particles are reflected from the fluid particle/wall collision plane according to the cosine law of diffuse scattering while simultaneously satisfying conditions corresponding to thermal equilibration with the solid surface. In MacElroy and Boyle, 1999, it was shown that in order to simulate equilibrated thermal scattering from a surface one need only sample three random numbers ξ_1, ξ_2, and ξ_3 uniformly distributed on {0,1} and compute the velocity components according to

$$v_1=v^*\cos(2\pi\xi_3)\sqrt{1-\xi_2} \quad (12a)$$

$$v_2=v^*\sin(2\pi\xi_3)\sqrt{1-\xi_2} \quad (12b)$$

$$v_3=v^*\sqrt{\xi_2} \quad (12c)$$

where the dimensionless speed $v^*=v\sqrt{m/2k_BT}$ is obtained from

$$\xi_1=(v^{*2}+1)\exp(-v^{*2}) \quad (12d)$$

v_1 and v_2 are the components of the velocity within the particle/wall scattering plane and v_3 is normal to this plane. This method ensures that the particles emanating from a plane are scattered with

a Maxwellian distribution of molecular speeds.

For hard core systems [Eq. (10a)] the application of this procedure involves a very simple modification of the Alder-Wainwright method [Alder and Wainwright, 1959] for tracking the fluid particle trajectories. Application of the technique for soft potentials [i.e. Eq. (10b)] is best illustrated as follows for the Verlet finite difference algorithm [Verlet, 1967]. This algorithm requires the initial centre of mass positions **r**, velocities **v** and accelerations **a** [based on force calculations using Eq. (10b)] of each particle i:

$$\mathbf{r}_i(\delta t)=\mathbf{r}_i(0)+\mathbf{v}_i(0)\delta t+\frac{1}{2}\mathbf{a}_i(0)\delta t^2 \tag{13a}$$

For times greater than this first step the particle positions are computed using

$$\mathbf{r}_i(t+\delta t)=2\mathbf{r}_i(t)-\mathbf{r}_i(t-\delta t)+\mathbf{a}_i(t)\delta t^2 \tag{13b}$$

with the velocity at time t given by

$$\mathbf{v}_i(t)=\frac{\mathbf{r}_i(t+\delta t)-\mathbf{r}_i(t-\delta t)}{2\delta t} \tag{13c}$$

As the particle trajectories evolve the momentum and kinetic energy of any given particle are changed randomly when the relative separation of the fluid particle and an atom of the solid corresponds to the location of the minimum, $r_{is}=2^{1/6}\sigma_{is}$, in the pair potential function. As discussed in MacElroy and Boyle, 1999, this is a fundamental requirement of the technique and therefore a procedure must be employed to determine, *a posteriori*, if, during a given time step, the relative separation of a fluid particle and a solid atom satisfies the condition $r_{is}=2^{1/6}\sigma_{is}$. If so, the particle trajectory is retraced to determine the point of 'collision' by using Newton's method to solve the expression

$$\left|\mathbf{r}_i(t)-\mathbf{r}_c+\mathbf{v}_i(t)f\delta t+\frac{1}{2}\mathbf{a}_i(t)(f\delta t)^2\right|^2=(2^{1/6}\sigma_{is})^2 \tag{14}$$

where $0<f<1$. Once the minimum value of f has been determined for a given i−s pair, particle i is advanced through time $f_{min}\delta t$ and its velocity components are changed according to the prescription described in Eq. (12). The completion of the time step is then achieved by moving the particle to

$$\mathbf{r}_i(t+\delta t)=\mathbf{r}_i(t+f\delta t)+\mathbf{v}_i^{scatt}(1-f)\delta t \tag{15}$$

where $\mathbf{v}_i^{scatt}$ is the post-collisional velocity of the scattered particle. This procedure is to be applied to each fluid particle independently during a given time step and, if necessary, repeated when multiple 'collisions' for the same particle are predicted to occur within the time step.

At the end of a time step in which a 'collision' or 'collisions' occurs between a fluid particle and a solid atom the Verlet algorithm [Eq. (13)] is restarted by computing the position at t using the approximation

$$\mathbf{r}_i(t)=\mathbf{r}_i(t+\delta t)-\mathbf{v}_i^{scatt}\delta t \tag{16}$$

This analysis is repeated for each time step and for as many time steps as may be required to reach and then sample the steady-state fluxes of the components in the system.

The steady-state fluxes are determined quite simply by monitoring the net transfer of particles across one or more planes within the system and/or by noting the net number of insertions or deletions in the control volumes on either side of the membrane during sequential periods of time. In the first case the steady-state flux in the z-direction is computed using

$$J_i^z=\frac{1}{A^{xy}}\frac{(N_i^+-N_i^-)}{\Delta t N_p} \tag{17a}$$

where N_i^+ and N_i^- are the total number of particles of component i which have drifted downstream and upstream, respectively, relative to all N_p planes of cross-section A^{xy} normal to the flow during a total observation time Δt. The second method for computing the steady-state flux employs the relation

$$J_i^z=\frac{1}{\gamma A^{xy}}\frac{([M_c-M_d]_i^I-[M_c-M_d]_i^{II})}{n\Delta t_{GC}} \tag{17b}$$

where M_c^k and M_d^k are the total number of particles created or destroyed by grand canonical events in control volume k during the time period $n\Delta t_{GC}$ and n is the total number of time steps Δt_{GC} monitored under steady-state conditions. The time element Δt_{GC} may or may not correspond to the MD time step δt (in the outline provided above, for example, Δt_{GC} corresponds to the time between updates in neighborhood lists). The factor γ is 2.0 if confining background walls of the type shown in Fig. 2 are used and is equal to 4.0 if periodic imaging is employed in the z-direction.

In addition to providing particle fluxes, the nonequilibrium simulations will also give full details of the species concentration profiles from which one may either determine global permeabilities or local transport coefficients. The former are easily defined by

$$P_i=J_i^z(2L)/(n_{B,i}^I-n_{B,i}^{II}) \tag{18}$$

where $n_{iB,i}^k$ is the concentration of component i in control volume k. The local transport coefficients will be specific to the constitutive equation assumed to describe the flow.

The capabilities of this procedure are best illustrated by examples and in the next section four case studies which have been investigated in detail by the author and coworkers will be described.

CASE STUDIES

1. Flow and Diffusion of Pure Materials in Membranes and Pores

The first study of this kind was reported in MacElroy, 1994, where the nonequilibrium MD technique was introduced. The primary purpose of this work was to ascertain the contribution of the convective shear flow term [which was omitted in Eq. (1) and corresponds to the last term in parenthesis in Eq. (19) below] to the isothermal flux of a pure dense fluid in the z-direction within a model microporous medium (see for example, Mason and Viehland, 1978; Mason and Malinauskas, 1983).

$$J^z=-\left(D_{OO}K+\frac{nk_BTB_o}{\eta}\right)\frac{d(p/k_BT)}{dz} \tag{19}$$

The term D_{oo} within the parenthesis of this equation is known as the viscous slip coefficient and is simply the diffusive flux contribution in Eq. (1) for a single component fluid. In the zero pressure (zero density) limit this term reduces to the Knudsen diffu-

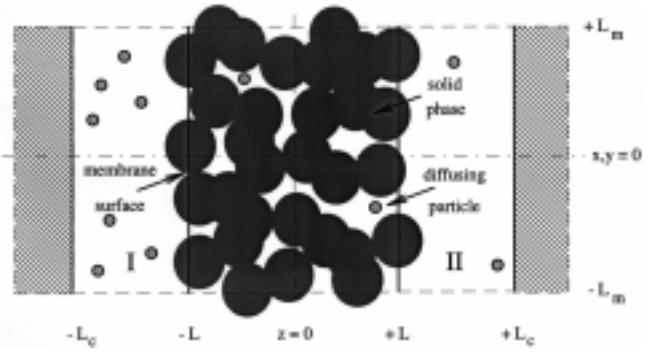

Fig. 3. Schematic diagram of the simulation cell for NEMD computations using the overlapping spheres membrane. The size of each control volume is $18\sigma_m^3$ and the mass transfer area is $9\sigma_m^2$ where σ_m is the diameter of one of the solid particles making up the membrane.

sion coefficient (hard core collisions) or 'activated' free particle diffusion coefficient (in the presence of a fluid/solid adsorption force field). The remaining parameters appearing in this equation are as follows: K is the equilibrium partition coefficient defining the local equilibrium distribution of the fluid within the porous medium relative to the bulk phase; n is the local pore fluid density; B_o is a medium structure factor associated with convective transport (typically proportional to the square of the average pore radius); and η is the shear viscosity of the pore fluid.

In MacElroy, 1994, a fluid composed of hard spherical particles, one of the simplest known fluids, was employed to investigate the properties of Eq. (19). The permeable medium considered in this work is shown schematically in Fig. 3 and consists of randomly overlapping spheres which are themselves impenetrable to the fluid particles. The control volumes I and II in these simulations extend over the entire fluid region to the left and to the right of the membrane. The membrane is generated by inserting spheres at random positions, selected using a uniform random number generator, in the volume between −L and +L. The fluid phase is created using the GCMC algorithm (in this case the simulations are comparatively straightforward since no potential energy changes need to be computed i.e. $\Delta\Phi_{\alpha\beta}$ only takes on one of two possible values, +∞ or 0.0) and the Alder-Wainwright [Alder and Wainwright, 1959] scheme for algebraically solving the equations of motion is readily applied to compute the particle trajectories.

Results for the permeabilities for three different cases and for a range of membrane thicknesses are illustrated in Fig. 4. In each case the membrane porosity is 0.5 and the fluid particles are one quarter the size of the membrane spheres. These conditions correspond qualitatively to transport of a simple fluid through a membrane containing pores in the range 1 to 2 nm i.e. typical of many microporous media employed in the chemical and process industries. While membranes as thin as the ones simulated are not usually encountered in practice the results do demonstrate conclusively that the viscous shear term appearing in Eq. (19) is negligible in comparison with the slip contribution. This is seen from the extrapolation of the results for finite systems to the left hand axis i.e. the infinite system, $1/(2L^*)\rightarrow 0$. The agreement between the extrapolated value and the exact value for the Knudsen

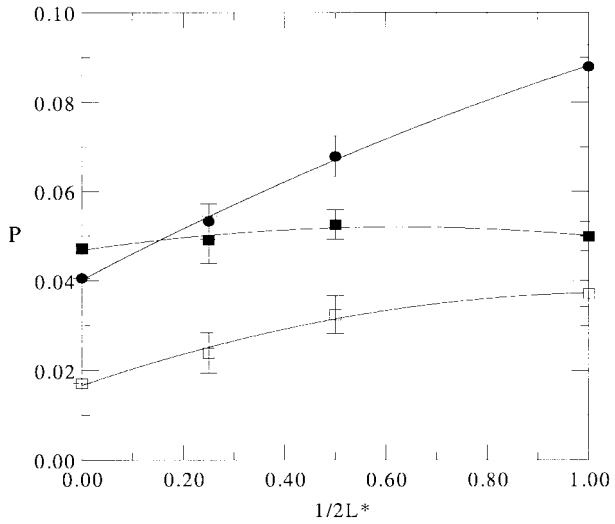

Fig. 4. The reduced permeability P, in units of $\sigma_m\sqrt{(k_BT/m)}$, as a function of the inversed thickness of the membrane with L^* in units of σ_m. (●) Ideal gas diffusion; (■) dense fluid flow (fluid particle/solid specular scattering); (□) dense fluid flow (fluid particle/solid diffuse elastic scattering).

(ideal gas) diffusion case (full circles) strongly supports the use of similar extrapolations for the dense fluid cases. In the latter simulations it was shown in MacElroy, 1994, that the pore fluid within the membranes is sufficiently dense to ensure that the transport process is in the transitional regime between the free particle and continuum limits. Under these conditions one might expect the viscous term in Eq. (19) to be of similar magnitude to the slip term however the data shown in Fig. 4 quite smoothly extrapolate to the value $D_{oo}K$ *alone* for the infinite system. The latter is computed from independent equililbrium molecular dynamics and GCMC simulations using periodically imaged 'infinite' systems of the same porosity as the membrane. The expression relating D_{oo} to the microscopic properties of the system (in this case fluctuations in the pore fluid centre of mass momentum) is [Suh and MacElroy, 1986]

$$D_{oo}=\frac{N}{3}\int_0^\infty \langle \mathbf{u}_o(t).\mathbf{u}_o(0)\rangle dt \qquad (20)$$

where N is the total number of fluid particles simulated in the EMD simulations and $\mathbf{u}_o$ is the centre of mass velocity for the pore fluid as a whole

$$\mathbf{u}_o(t)=\sum \mathbf{v}_i(t)/N$$

While the model system investigated in MacElroy, 1994, is very simple additional work reported in [Travis and Gubbins, 1999] supports the basic premise that shear flow effects are negligible within nanopore structures. This considerably simplifies the analysis of flows in such systems since only the slip terms need to be estimated. This particular issue will be revisited in Section 3.2 below.

The second case study involves a simple though nontrivial demonstration of single-file diffusion in pores of finite and infinite length [MacElroy and Suh, 1997a, b]. Single-file diffusion arises when the particles confined to a pore cannot overtake one another and is observed in biological systems (for example, ion transport

in protein forming membrane pores) and in a number of zeolitic materials depending on the size of the diffusant (Theta-1 zeolite [Barri et al., 1984], mordenite [Lei and Sachtler, 1993], and $AlPO_4$-5 [Gupta et al., 1995]). If the pores are infinitely long it may be shown theoretically [Levitt, 1973; Karger et al., 1992; Hahn and Karger, 1996] that the mean square displacement of a tracer particle (trace or self-diffusion conditions) is not linear in time but varies as $\sqrt{t}$ i.e.

$$\lim_{t\to\infty}\langle\Delta z^2(t)\rangle=2F\sqrt{t} \tag{21}$$

where F is the mobility

$$F=\frac{1-\rho\sigma}{\rho}\sqrt{\frac{D_{1d}(0)}{\pi}} \tag{22}$$

In this last expression ρ is the linear density of the fluid within the one-dimensional pore and $D_{id}(0)$ is the diffusivity at zero pore loading. Eq. (21) is strictly only true for random (diffuse) scattering of the fluid particles from the confining pore walls and while this should be the prevalent mode of particle/wall reflection in real systems, if specular (mirror image) scattering takes place then a linear relation between $\langle\Delta z^2(t)\rangle$ and time will be observed [Lebowitz and Percus, 1967; MacElroy and Suh, 1997a].

The diffusion process implied by Eq. (21) is clearly non-Fickian [i.e. diffusion is not defined in the stationary infinite time limit as may be seen by employing Eq. (2b) with Eq. (21)]. However in real single-file biological and zeolitic systems trace diffusion is widely acknowledged to take place for the simple reason that real pores are finite in length. This was demonstrated theoretically for the first time in MacElroy and Suh, 1997a using the NEMD technique. In this study a simplified model based on 'colour' particle diffusion within cylindrical pores (see Fig. 5) was employed to demonstrate the distinction between single-file pores of infinite and finite length. The diffusing particles were hard spheres whose diameter, σ, was greater than the radius of the pore thus ensuring the absence of overtaking trajectories within the pore. The NEMD simulations were conducted from an initial state in which light 'grey' particles and dark 'grey' particles fully occupied the left and right hand sides of the simulation cell, respectively, as illustrated in Fig. 5. The only difference between the particles is their 'colour' and there is no overall density difference between the left and right hand sides of the cell at the beginning or during the period of the simulation. As the simulation progresses the light particles will on average diffuse from control volume I to II and the dark particles will be transported in the opposite direction. The steady-state concentration gradients are achieved by maintaining the chemical potentials of the particles of different 'colour' at high or low values within the respective control volumes while keeping the fluid densities in both volumes equal.

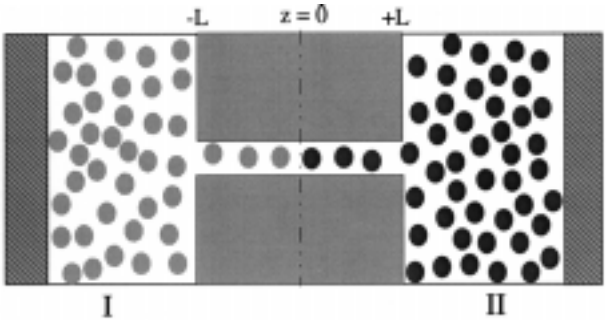

Fig. 5. Schematic diagram of the simulation cell for NEMD computations of single file diffusion. The volumes of regions I and II are both chosen to be equal to $VL_xL_yL_z=(5\sigma)(5\sigma)(8\sigma)$ (σ is the fluid particle diameter) and are periodically imaged in the x and y directions.

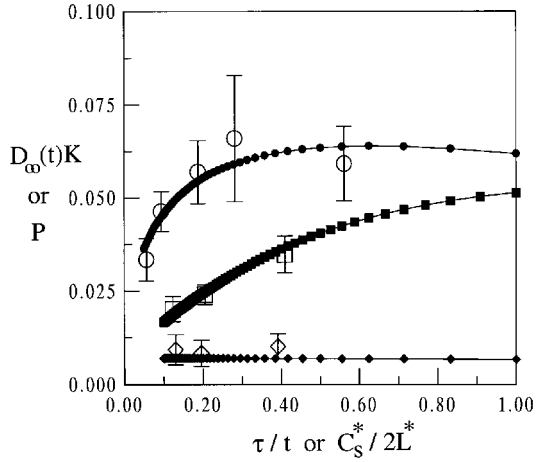

Fig. 6. The time-dependent permeability, $D_\infty(t)K$, for pores of infinite length at short times as a function of τ/t (filled symbols), and the steady-state permeability for finite length pores, P, as a function of $C_s^*/2L^*$ (open symbols) for pores with diffusely reflecting walls. The time dependent diffusion coefficient $D_\infty(t)$ is in units of $R_P\sqrt{(3k_BT/m)}$ and $\tau=R_P/\sqrt{(3k_BT/m)}$. C_s^* is the dimensionless speed of sound within the pore in units of $\sqrt{(3k_BT/m)}$ and L^* is in units of R_P. ●$\sigma/2R_p=0.7$, $n_B^*=0.4$, K=0.524, $F^*=0.670$; ■$\sigma/2R_p=0.7$, $n_B^*=0.6$, K=0.724, $F^*=0.148$; ◆$\sigma/2R_p=0.9$, $n_B^*=0.4$, K=0.122, $F^*=5.07$; where $n_B^*=n\sigma^3$, $F^*=F\sqrt{\tau/R_p^4}$ and K is the equilibrium partition coefficient $K=n_P/n_B$.

The results obtained for a range of pore lengths, two pore radii and two fluid densities are reproduced in Fig. 6. In this figure we have simultaneously plotted (i) the permeability P against inverse pore length in the form $C_s^*/2L^*$ where C_s^* is the dimensionless speed of sound in the one-dimensional pore fluid and (ii) the time-dependent permeability for a pore of infinite length as a function of inverse reduced time τ/t. The filled symbols in this figure were obtained from EMD simulations for a pore of infinite length and the long time value for $D_\infty(t)$ in each case is predicted by Eq. (21) to be $F/(2\sqrt{t})$. These results demonstrate not only that diffusion in finite length single-file pores exists but also that, in scaling the pore length with the speed of sound, the data sets for both the NEMD (finite pore length) and EMD (infinite length pore) simulations collapse onto one another. In MacElroy and Suh, 1997b, this was explained in terms of decorrelation times associated with the rate at which a sound wave travels along the single file of fluid particles. For long pores the correlated dynamics of the pore fluid particles persist to long times and the influence of the random motion within the reservoirs in volumes I and II only enters at times corresponding to $2L^*/C_s^*$. By inference, it also follows that this correspondence between spatial and temporal length scales leads to the following simple expression for the Fickian diffusion coefficient in single-file pores of finite length

$$\lim_{L\to\infty} D = \frac{F}{2}\sqrt{\frac{C_s}{2L}} \qquad (23)$$

i.e. D scales as $1/\sqrt{L}$ in long single-file pores. The more general result implied by the data shown in Fig. 6 is that the effective Fickian diffusion within pores of arbitrary length is readily obtained from a *single* trajectory computation for a pore of infinite length.

2. Separation of Binary Mixtures using 'Thin' Microporous Membranes

While the simulations described in section 3.1 demonstrate specific aspects of the underlying philosophy of the NEMD method, processes which might be considered to be of more immediate chemical engineering interest have also been investigated in MacElroy et al., 1999, and MacElroy and Boyle, 1999. In the first of these studies [MacElroy et al., 1999] the kinetic separation of air into its constituents using carbon molecular sieves (CMSs) [Chihara et al., 1978; Chihara and Suzuki, 1979; Ruthven et al., 1986; Ruthven, 1992; Kikkinides et al., 1993; Chen et al., 1994] was examined in some detail. The physical mechanism controlling this particular separation is believed to be associated with very small apertures within the CMS medium as depicted schematically in Fig. 7. It is known (see for example, Moore and Trimm, 1977) that by gradually depositing carbonaceous material on the surface of the pores within a carbon substrate the aperture narrows and ultimately pore widths close to the kinetic diameters of nitrogen and oxygen are created within the CMS medium. In MacElroy et al., 1999, it was shown using NEMD that, although pore narrowing is an important issue (see MacElroy et al., 1997, for further details on this aspect of the problem), it is in fact the increase in nanopore *length* during the deposition process which controls CMS kinetic selectivity.

In order to simulate the permeation characteristics of nitrogen and oxygen within a single aperture of the kind illustrated in Fig. 7, MacElroy et al., 1999, employed the model 'membrane' system shown in Fig. 8(a). The permeable medium in this case is a single heterogeneous carbon pore generated by randomly etching the graphite basal planes on either side of a slit-like cavity as illustrated in Fig. 8(b). The etched pore walls employed in this work are considered to be analogous to pore surfaces generated by carbon deposition (further details are provided by MacElroy et al., 1997). By varying the degree of etching, or adjusting the

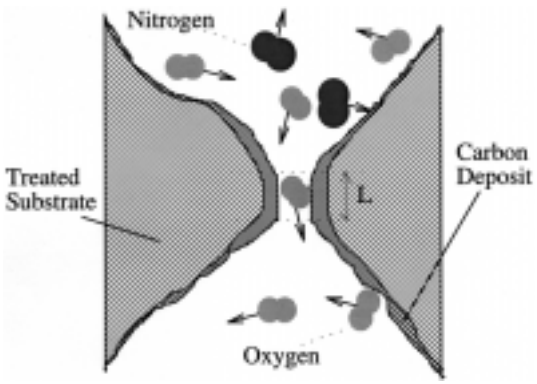

Fig. 7. Schematic representation of the influence of carbon deposition on the oxygen/nitrogen selectivity of a pore mouth in carbon molecular sieve.

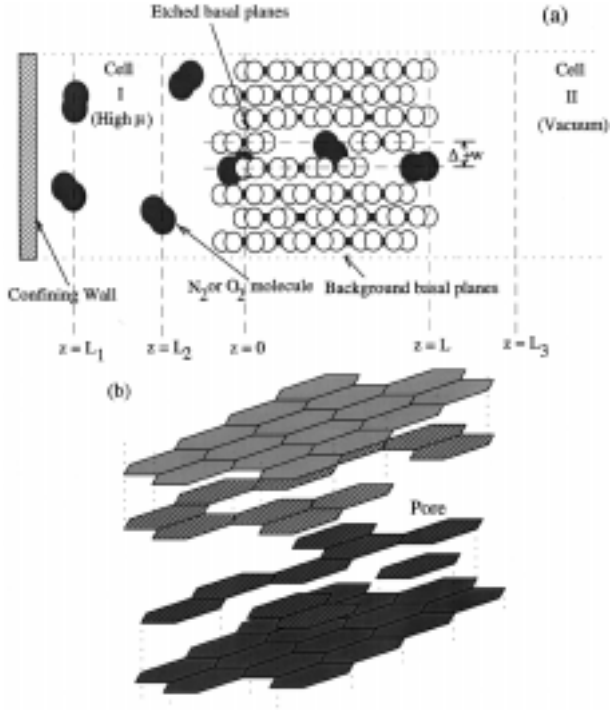

Fig. 8. (a) Side view of the carbon membrane for the case L= 8l_{cc} (where l_{cc}=0.142 nm) and w=0 (Δ=0.335 nm); (b) Schematic diagram of a carbon slit pore with etched graphitic walls.

distance between these walls and/or changing the length L of the pore it is possible to investigate a wide range of 'aperture' conditions which may directly influence the selectivity of CMS. Following prior work reported in MacElroy et al., 1997, and Seaton et al., 1997, which concluded that pore width alone could not reproduce experimental observations (most notably the magnitude of the experimental diffusivities of N_2 and O_2), it was decided in MacElroy et al., 1999, to focus attention on the pore length and degree of etching. To simplify the NEMD computations while retaining the most important features of the separation process, the gas phase in chamber I was treated as ideal (the fugacity of the gas in the control volume is simply its partial pressure) and a vacuum was employed in chamber II (i.e. any gas molecules reaching z=L_3 were immediately deleted from the list of gas particles in the system). Also, since the structure of the N_2 and O_2 molecules is an important factor in the air/CMS separation process, the gas molecules were treated as diatomic particles in the simulations and therefore in addition to solving the centre-of-mass equations of motion of the molecules it was necessary to include the reorientational dynamics of the diatoms [Fincham, 1984].

The results reported by MacElroy et al., 1999, demonstrated that of the two possibilities (i) degree of etching (or deposition density) and (ii) pore length, only the latter has a direct influence on the selectivity of the CMS. To illustrate this the results for the three longest pores investigated in this work are shown in Fig. 9 for two pore widths w as defined in Fig. 8 (in all of these simulations the degree of etching was 40%). In all cases the quantity P/L (in the current notation) is exponentially related to the pore length (rather than inversely proportional to L which one would

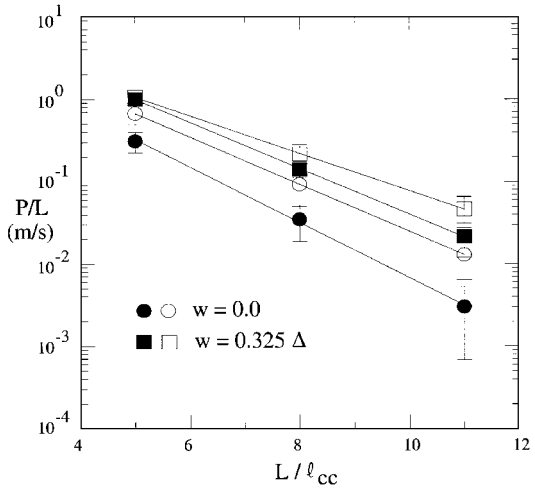

Fig. 9. Permeability as a function of carbon membrane thickness with 40% etching. The filled and open symbols are for nitrogen and oxygen respectively.

expect for Fickian diffusion conditions) and this dependence was shown by MacElroy et al., 1999, to be due to non-Fickian diffusion of the kind discussed earlier with reference to Fig. 1(b). Based on a theoretical analysis of transport within a random medium containing pore clusters which, on average, are percolating only over a limited spatial range λ_i, it was shown that the permeability may be simply expressed as

$$\frac{L}{p_i}=\left(\frac{1}{K_{I,i}}+\frac{1}{k_{II,i}\exp(-L/\lambda_i)}\right) \tag{24}$$

where $k_{I,i}$ and $k_{II,i}$ are gas phase rate coefficients for transport to the membrane face in chamber I and from the membrane face in chamber II. The pore cluster spatial range λ_i is specific to the component and is *very* sensitive to the diameter of the diffusing molecule. For example for the pore width w=0.325Δ the values obtained for this parameter for nitrogen and oxygen were 0.222 nm and 0.273 nm, respectively, while the individual atomic diameters within the diatoms of N_2 and O_2 are 0.3296 nm and 0.294 nm.

A comparative analysis of the simulation results and experimental data for Takeda CMS [Chihara et al., 1978a, b] and Bergbau-Forschung CMS [Chen et al., 1994] is provided in Fig. 10. The selectivity, defined by $R=D_{O_2}/D_{N_2}$, computed using the relation

$$D_i=\frac{k_{II,i}L}{K_i}\exp(-L/\lambda_i) \tag{25}$$

and the simulation results, is plotted in Fig. 10(a) as a function of pore length for both of the pore widths reported in Fig. 9. The selectivities cited in the literature for Takeda CMS and Bergbau-Forschung CMS are 3.1 and 36.0 respectively and from Fig. 10(a) this suggests that the average aperture length within these materials is approximately 1.7 nm for Takeda CMS and 4.7 nm for Bergbau-Forschung for pore widths w defined in Fig. 8 in the range 0.0 to 0.11 nm. Fig. 10(b) demonstrates that this model can provide accurate estimates of the widely disparate diffusivities observed for these materials. The results for the pore width w=0.325Δ are in fact only a factor of 7 lower for the Takeda CMS (experimental value $D_{O_2}=6.7\times10^{-11}$ m^2/s) while the simulation

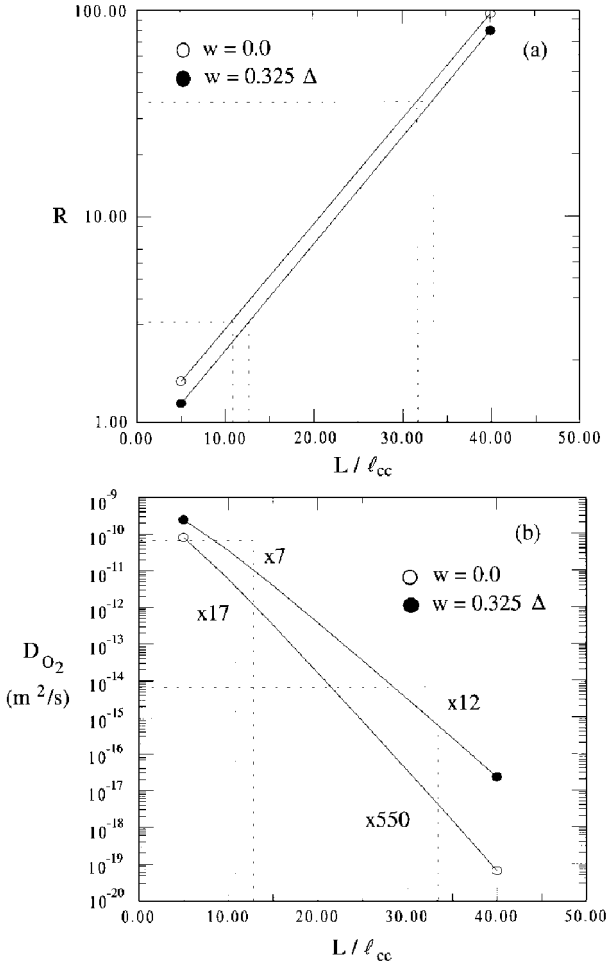

Fig. 10. (a) Diffusivity ratio $R=D_{O_2}/D_{N_2}$ as a function of pore length. The horizontal dotted lines correspond to the experimental values for Takeda CMS (3.1) and Bergbau-Forschung CMS (36). (b) The oxygen diffusivity as a function of pore length. The horizontal dotted lines correspond to the experimental values for Takeda CMS (6.7×10^{-11} m^2/s) and Bergbau-Forschung CMS (6.5×10^{-15} m^2/s).

results are lower by a factor of 12 for the Bergbau-Forschung CMS ($D_{O_2}=6.7\times10^{-15}$ m^2/s). One can quite easily envisage that a small increase in the pore width and aperture length could lead to excellent agreement. Additional work reported in MacElroy et al., 1999, also demonstrates that the same conclusions are arrived at even if a distribution of pore sizes is taken into consideration.

It is also important to note that while only carbon molecular sieves were considered by MacElroy et al., 1999, it is clear that the physical principles revealed in this work may be readily applied to other systems (for example, controlled chemical vapour deposition of silica on amorphous silica substrates [Tsapatsis and Gavalas, 1992, 1997]). Tailoring amorphous nanoporous systems in this manner to achieve both kinetic as well as adsorptive selectivity opens up a wide variety of possibilities for separating 'difficult' mixtures.

In the final case study [MacElroy and Boyle, 1999] the carbon membrane simulated is very similar to the structure shown in Fig. 8 with the simplification that no etching is involved. The pur-

pose of this investigation was to examine the adsorptive selectivity of dense gas mixtures and, in particular, to verify the hypothesis that for H_2/hydrocarbon separations it is hydrocarbon pore filling which accounts for hydrogen enrichment on the high pressure side during membrane separations of these mixtures. Additional issues under consideration in this work were (a) the validity of Fickian flux expressions for diffusion within very narrow but open (fully percolating) pores; (b) the relative magnitude of the cross-coupling terms appearing in the flux equations predicted both by nonequilibrium statistical mechanics and irreversible thermodynamics [the terms $i \neq j$ in Eqs. (1) and (8)]; (c) the relative contribution of the mass transfer resistance at the pore entrance/exit for adsorbing dense fluid mixtures; and (d) the magnitude of the viscous term in the species transport equations [i.e. the second term in Eq. (19) which, for multicomponent mixtures, appears in Eq. (1) in precisely the same form except n_i replaces n and η is understood to be the pore fluid mixture viscosity].

In the system investigated by MacElroy and Boyle, 1999, a single graphitic pore width of $w=1.25\Delta$ (see Fig. 8) was employed in the simulations and the permeation characteristics of H_2/CH_4 mixtures were investigated for (a) pressure driven transport from control volume I to control volume II (two separate sets of simulations were conducted for both gases) and (b) isobaric counterdiffusion of the two components. The temperature employed in the simulations was 0 °C in all cases and the permeabilities were computed for a range of pore lengths L. In this case the definition of the permeability differs from Eq. (18) in that the concentration $n_{B,i}$ is replaced by the fugacity $\hat{f}_i^I$ and $\hat{f}_i^{II}$, i.e.

$$P_i = J_i^z(2L)/(\hat{f}_i^I - \hat{f}_i^{II}) \tag{26}$$

This simplifies the comparison between the NEMD results and independent computations conducted using EMD and Eq. (2) on an 'infinitely' long pore.

The principal results of this work are shown in Figs. 11-13. The permeabilities under forced flow conditions cited in Fig. 11(a) refer to two independent sets of computations in which a chemical potential gradient was maintained for only one of the components. In conjunction with subsidiary results (the absence of fluxes for the species whose fugacity is maintained constant) the following conclusions were arrived at:

(i) The cross-coupling terms D_{ij} and the viscous flow terms in Eq. (1) do not influence the fluxes under forced flow conditions. If one or both these contributions did play a role then, as Eqs. (1) suggests, transport of the material maintained at fixed chemical potential would have been observed. This conclusion is supported by the local (pore centreline, z=0) effective diffusivities shown in Fig. 13(a) which were computed from the concentration gradients (and hence the chemical potential gradients), some of which are provided in Fig. 12(a). The horizontal dashed lines in Fig. 13(a) tagged by open and filled squares are the infinite system direct diffusivities D_{ii} for both species.

(ii) The predicted results for the permeabilities in an infinite pore under forced flow conditions are also shown in Fig. 11(a) as horizontal dashed lines and it is clear that the much lower methane permeabilities for pores of finite length (filled circles) arise due to significant pore entrance/exit mass transfer resistances. The short dashed curve traced through these points actually corresponds

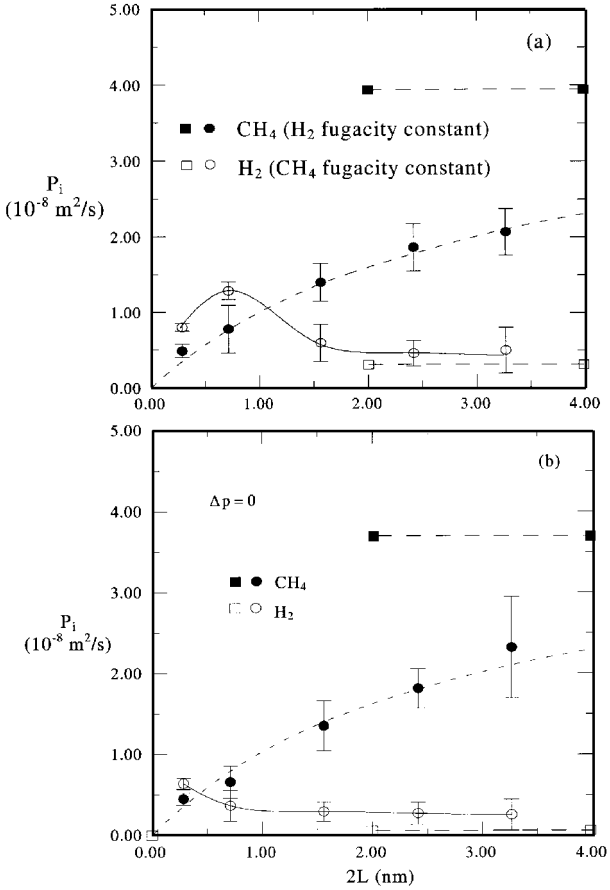

Fig. 11. NEMD methane and hydrogen permeabilities obtained from (a) pressure driven transport and (b) isobaric counterdiffusion. The dashed lines tagged by open and filled squares correspond to the predicted results for infinitely long pores and the dashed line through the filled circles corresponds to Eq. (27).

to

$$\frac{1}{P_{CH_4}} = \frac{1}{P^o_{CH_4}\cdot(2L)} + \frac{1}{P^p_{CH_4}} \tag{27}$$

where $1/P^o_{CH_4}$ represents the resistance at the pore ends and $P^p_{CH_4}$ is the intrapore permeability which, for fully percolating pores, should, in principle, be independent of pore length. The results shown in Fig. 11(a) imply that the influence of the pore ends will be negligible (<1%) only if this comparatively narrow pore is of the order of 0.1 microns or greater in length. The significant affect of the pore entrance/exit on transport of methane has also been observed in very recent work by Nitta and Furukawa, 1999.

(iii) The hydrogen permeabilities in Fig. 11(a) display a maximum which is characteristic of pore blockage by the methane as the pore length (and hence adsorptivity of methane) is increased. As the pore length increases it is observed that the separation selectivity of the carbon pore for methane over hydrogen approaches 10 which is typical of real experimental data reported in the literature (see, for example, Rao and Sircar, 1993). Similar results have been reported by Furukawa and Nitta, 1997, in their studies of ethane/methane separation using model carbon pores.

(iv) The results shown in section (b) of Figs. 11 to 13 repre-

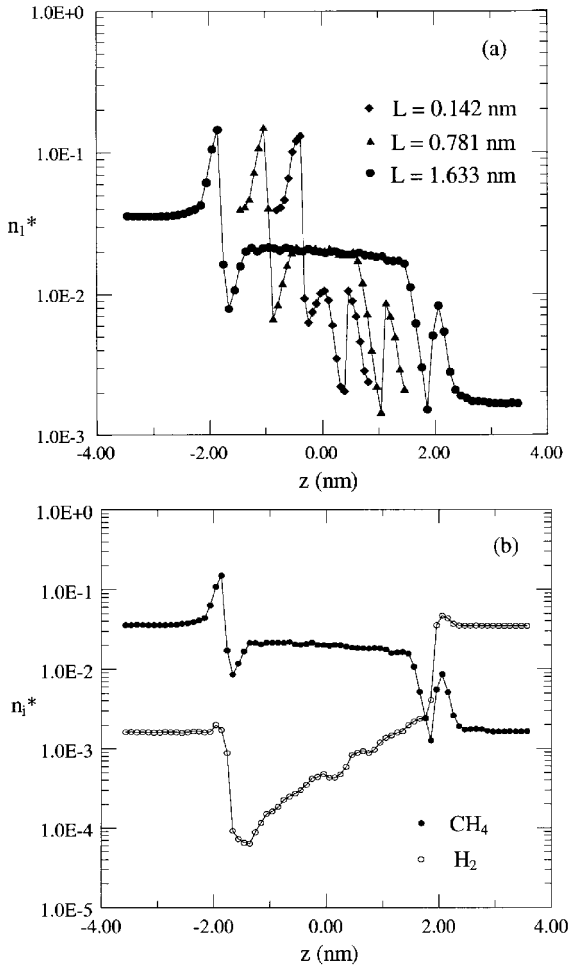

Fig. 12. Concentration profiles through the pores (n^* is the reduced density in units of Δ^{-3}). (a) Methane density profiles for three pore lengths under forced flow conditions (fixed H_2 fugacity); (b) Methane and hydrogen profiles within the pore of length 2L=3.266 nm under isobaric conditions.

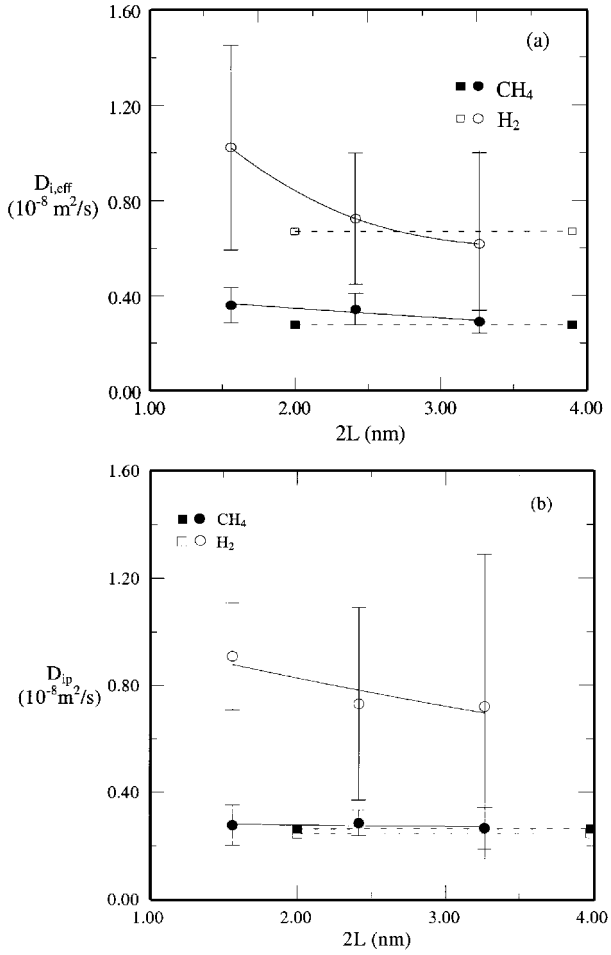

Fig. 13. Centreline diffusivities for the three longest pores as functions of pore length. (a) Effective diffusivities, $D_{i,eff}$, for methane and hydrogen under forced flow conditions; (b) Pore diffusivities under isobaric conditions.

sent isobaric counterdiffusion of methane and hydrogen. The general trends are very similar to the forced flow results with two exceptions: the overall hydrogen transport is significantly reduced [compare the open symbol data shown in Figs. 11(a) and 11(b)] while the magnitude of the pore centreline effective diffusivity is much larger than the value predicted for a pore of infinite length (Fig. 13). The permeability reduction is due to pore blockage at the methane upstream end of the pore where the loading is significantly higher than in the forced flow simulations at uniform methane chemical potential. The results for the centreline hydrogen diffusivity, however, are not as easily interpreted. The predicted value for the diffusivity within the infinite length pore [dashed line tagged by open squares in Fig. 13(b)] is approximately a factor of three lower than the value shown in Fig. 13(a) for forced flow and MacElroy and Boyle, 1999, have demonstrated that this is due to an important contribution to the counterdiffusing hydrogen flux arising from the cross term D_{ij} ($i \neq j$) (the methane flux is largely unaffected). For the finite length pore we can only suggest at this time that in view of the similarity of the magnitude of the centreline hydrogen diffusivities in both the forced flow and isobaric simulations, coupling near the pore centreline in the short pores is not significant and this raises serious questions concerning the validity of Eq. (1) in its application to nonadsorbing or weakly adsorbing gases in pores of finite spatial range (nonlocal dependencies of the kind indicated in Eq. (8) should be taken into consideration for such gases). In contrast it would appear that the stationary 'infinite' system flux equations are valid for strongly adsorbing species due to rapid decorrelation of the time correlation functions as the adsorbing molecule is scattered repeatedly over short distances within and between the adsorption sites on the solid surface.

RELATED WORK AND FUTURE DIRECTIONS

The computational facilities required to conduct simulations of the kind described in section 3 are not resource demanding in view of the current availability of comparatively low cost workstations or personal computers. For example, typical run times for the case studies cited in Section 3.2 were between 5 and 20 picoseconds of trajectory time per minute of CPU time on a dedicated (serial) Digital 433au series workstation. These computations usually involved approximately 300 fluid particles and over

1000 carbon substrate atoms. From an applications point of view, single nanopore or micropore simulations of this type provide fundamental information which may be used in conjunction with an appropriate network model of the pore space to obtain an accurate model for transport within a given porous medium (see for example, Sahimi, 1994). There are limitations, however, and important questions may arise if pore junctions are deemed to influence transport within the network. If this should prove to be the case, then analysis at the single pore level will need to be supplemented with simulations of pore-pore correlation effects under *nonequilibrium* conditions. Studies of this kind are currently in progress [Xu et al., 1999] and it is anticipated that, by incorporating such effects into network models, a powerful predictive tool, requiring only limited information on a particular pore structure, will result.

As illustrated in the first case study in section 3.1 one is not restricted to single pore structures and systems of effectively 'infinite' range may be investigated by introducing periodic boundary conditions in the z-direction (i.e. removing the optional walls shown in Fig. 2) and extending the pore structure throughout the entire volume (including the control volumes I and II). If necessary, much larger model systems may be studied over significantly longer periods of time by making use of the parallel computing facilities provided by microprocessor clusters or supercomputers. The latter approach has been particularly emphasised in recent work by Heffelfinger and coworkers [Pohl et al., 1996; Heffelfinger and Ford, 1998; Ford and Heffelfinger, 1998; Thompson et al., 1998; Pohl and Heffelfinger, 1999; Thompson and Heffelfinger, 1999]. A number of important problems are tackled in these studies, including transport within polymeric media (with the intramolecular dynamics of the polymer chains included in the simulations) [Ford and Heffelfinger, 1998] and transport of a large molecular species [Thompson and Heffelfinger, 1999]. This latter study is of significance in that it reports a novel algorithm to overcome difficulties associated with the GC creation/destruction phase of the NEMD method. GC creation/destruction steps are subject to one major drawback, namely, the very low probability of finding a cavity of sufficient size to insert a particle when the particle is large or the fluid density is high (creation step) or the very low probability of generating a cavity in a fluid during an attempted removal of a particle also when the particle is large or the fluid density is high (destruction step). Thompson and Heffelfinger, 1999, avoid this problem by conducting the simulations at fixed temperature and pressure (rather than fixed volume) while simultaneously maintaining fixed chemical potentials for all of the species except one (the large particle component) within the respective control volumes. The number of particles of the large species is maintained constant during the simulations. This procedure should be of particular value in simulations involving large hydrocarbon molecules during separation of petrochemical mixtures or transport of biospecies across model biological membranes. In future work on systems of the latter kind it is also possible that algorithmic developments in the simulation of rare event dynamics (see for example Ànderson, 1995; Tunca and Ford, 1999) or 'hyper' molecular dynamics [Voter, 1997] could play an important role in tracking the temporal evolution of the particle trajectories. This will require a careful assessment of these techniques in their ability to simulate the collective modes of the transport process.

NOMENCLATURE

a : acceleration [m/s^2]
B_o : viscous flow coefficient [m^2]
C(t) : velocity correlation function [m^2/s^2]
C_s : speed of sound [m/s]
D : diffusion coefficient [m^2/s]
F : single-file mobility [m^2/$\sqrt{s}$]
$\hat{f}$: fugacity [J/(mole·m^3)]
J, **J** : flux [particles/m^2·s]
j : microscopic particle current [particles/m^2·s]
K : equilibrium partition coefficient
k_B : Boltzmanns constant
$k_{m,i}$: membrane surface mass transfer coefficient [m/s]
k : wave vector [m^{-1}]
L : pore half-length or total pore length in the etched carbon membranes [nm]
L_{ij} : phenomenological coefficient [s/kg·m^2]
m : particle mass [kg]
n : particle number density [particles/m^3]
N : particle number
p : pressure [N/m^2]
P : permeability [m^2/s]
P^o : pore mouth conductance [m/s]
P^p : intrapore permeability [m^2/s]
R : oxygen/nitrogen diffusivity ratio
r_{ij} : relative separation of particles i and j [nm]
r : particle coordinate [m]
t : time [s]
T : temperature [K]
$\mathbf{u}_o$: fluid centre of mass velocity [m/s]
v : particle velocity [m/s]
V : volume [m^3]
w : pore width [nm]
x, y, z: cartesian coordinates [m]

Greek Letters

Δ : interplane spacing in graphite [0.335 nm]
ε : potential minimum in the Lennard-Jones (12-6) potential function [J/particle]
η : shear viscosity [N·s/m^2]
μ : chemical potential [J/particle]
ξ : uniformly distributed random number
ρ : single-file number density [particles/nm]
σ : Lennard-Jones (12-6) diameter or hard sphere diameter [nm]
ϕ : potential interaction energy [J]
Φ : system potential energy [J]
ω : frequency [s^{-1}]
λ : average percolation cluster size [nm]
l_{cc} : carbon-carbon bond length in graphite [0.142 nm]

Subscripts

B : bulk fluid state

I : cell I
II : cell II
i : species or particle index
j : species or particle index

REFERENCES

Adams, D. J., "Chemical Potential of Hard Sphere Fluids by Monte Carlo Methods," *Mol. Phys.*, **28**, 1241 (1974).

Adams, D. J., "Grand Canonical Ensemble Monte Carlo for a Lennard-Jones Fluid," *Mol. Phys.*, **29**, 307 (1975).

Alder, B. J. and Wainwright, T. E., "Studies in Molecular Dynamics. I. General Method," *J. Chem. Phys.*, **31**, 459 (1959).

Allen, M. P. and Tildesley, D. J., "Computer Simulation of Liquids," Clarendon, Oxford (1987).

Altenberger, A. R., Dahler, J. S. and Tirrell, M., "On the Molecular Theory of Diffusion and Heat Conduction in Multicomponent Solutions," *J. Chem. Phys.*, **86**, 2909 (1987).

Anderson, J. B., "Predicting Rare Events in Molecular Dynamics," *Adv. Chem. Phys.*, **91**, 381 (1995).

Barri, S. A. I., Smith, G. W., White, D. and Young, D., "Structure of Theta-1, the First Unidimensional Medium-pore High-silica Zeolite," *Nature*, **312**, 533 (1984).

Berne, B. J., "Time-Dependent Properties of Condensed Media," Ch. 9 in Physical Chemistry-An Advanced Treatise, **8B**, D. Henderson, (Ed.), Academic press (1971).

Chen, Y. D., Yang, R. T. and Uawithya, P., "Diffusion of Oxygen, Nitrogen and their Mixtures in Carbon Molecular Sieve," *AIChE J.*, **40**, 577 (1994).

Chihara, K., Suzuki, M. and Kawazoe, K., "Interpretation for the Micropore Diffusivities of Gases in Molecular-Sieving Carbon," *J. Colloid Interface Sci.*, **64**, 584 (1978a).

Chihara, K., Suzuki, M. and Kawazoe, K., "Adsorption Rate on Molecular Sieving Carbon by Chromatography," *AIChE J.*, **24**, 237 (1978b).

Chihara, K. and Suzuki, M., "Control of Micropore Diffusivities of Molecular Sieving Carbon by Deposition of Hydrocarbons," *Carbon*, **17**, 339 (1979).

Cracknell, R. F., Nicholson, D. and Quirke, N., "Direct Molecular Dynamics Simulation of Flow Down a Chemical Potential Gradient in a Slit-shaped Micropore," *Phys. Rev. Lett.*, **74**, 2463 (1995).

Fincham, D., "More on Rotational Motion of Linear Molecules," *CCP5 Quarterly*, **12**, 47 (1984).

Ford D. M. and Glandt, E. D., "A Molecular Simulation Study of the Surface Barrier Effect: Dilute Gas Limit," *J. Phys. Chem.*, **99**, 11543 (1995).

Ford, D. M. and Heffelfinger, G. S., "Massively Parallel Dual Control Volume Grand Canonical Molecular Dynamics with LADERA. II. Gradient-driven Diffusion through Polymers," *Mol. Phys.*, **94**, 673 (1998).

Furukawa, S., Shigeta, T. and Nitta, T., "Nonequilibrium Molecular Dynamics for Simulating Permeation of Gas Mixtures through Nanoporous Carbon Membranes," *J. Chem. Eng. Japan*, **29**, 725 (1996).

Furukawa, S. and Nitta, T., "Computer Simulation Studies on Gas Permeation through Nanoporous Carbon Membranes by Nonequilibrium Molecular Dynamics," *J. Chem. Eng. Japan*, **30**, 116 (1997).

Gefen, Y., Aharoni, A. and Alexander, S., "Anomalous Diffusion on Percolating Clusters," *Phys. Rev. Lett.*, **50**, 77 (1983).

Green, M. S., "Markoff Random Processes and the Statistical Mechanics of Time Dependent Phenomena," *J. Chem. Phys.*, **20**, 1281 (1952).

Green, M. S., "Markoff Random Processes and the Statistical Mechanics of Time Dependent Phenomena. II. Irreversible Processes in Fluids," *J. Chem. Phys.*, **22**, 398 (1954).

Gupta, V., Nivarthi, S. S., McCormick, A. V. and Davis, H. T., "Evidence for Single-file Diffusion of Ethane in the Molecular Sieve AlPO4-5," *Chem. Phys. Lett.*, **29**, 596 (1995).

Haberlandt, R. and Karger, J., "Molecular Dynamics under the Confinement by the Host Lattice in Zeolitic Adsorbate-Adsorbent Systems," *Chem. Eng. J.*, **74**, 15 (1999).

Hahn, K. and Karger, J., "Molecular Dynamics Simulation of Single-file Systems," *J. Phys. Chem.*, **100**, 316 (1996).

Heffelfinger, G. S. and Ford, D. M., "Massively Parallel Dual Control Volume Grand Canonical Molecular Dynamics with LADERA. I. Gradient-driven Diffusion in Lennard-Jones Fluids," *Mol. Phys.*, **94**, 659 (1998).

Heffelfinger, G. S. and van Swol, F., "Diffusion in Lennard-Jones Fluids using Dual Control Volume Grand Canonical Molecular Dynamics Simulation (DCV-GCMD)," *J. Chem. Phys.*, **100**, 7548 (1994).

Karger, J., Petzold, M., Pfeifer, H., Ernst, S. and Weitkamp, J., "Single-file Diffusion and Reaction in Zeolites," *J. Catal.*, **136**, 283 (1992).

Kaufman, T. G. and Leonard, E. F., "Studies in Intramembrane Transport: A Phenomenological Approach," *AIChE J.*, **14**, 110 (1968).

Kikkinides, E. S., Yang, R. T. and Cho, S. H., "Concentration and Recovery of CO_2 from Flue Gas by Pressure Swing Adsorption," *Ind. Eng. Chem. Res.*, **32**, 2714 (1993).

Kubo, R., Toda, M. and Hashitsume, N., "Statistical Physics II. Nonequilibrium Statistical Mechanics," Springer-Verlag, Berlin (1985).

Lebowitz, J. L. and Percus, J. K., "Kinetic Equations and Density Expansions: Exactly Solvable One-dimensional System," *Phys. Rev.*, **155**, 122 (1967).

Lei, G.-D. and Sachtler, W. M. H., "H D Exchange of Cyclopentane on Pt Mordenites-Probing for Monatomic Pt Sites," *J. Catal.*, **140**, 601 (1993).

Levitt, D. G., "Dynamics of a Single-file Pore: Non-Fickian Behaviour," *Phys. Rev. A*, **8**, 3050 (1973).

MacElroy, J. M. D. and Suh, S.-H., "Computer Simulation of Moderately Dense Hard-Sphere Fluids and Mixtures in Microcapillaries," *Mol. Phys.*, **60**, 475 (1987).

MacElroy, J. M. D., "Diffusion in Homogeneous Media," Ch. 1 in Diffusion in Polymers, Neogi, P. (Ed.) Marcel Dekker, New York (1997).

MacElroy, J. M. D., "Nonequilibrium Molecular Dynamics Simulation of Diffusion and Flow in Thin Microporous Membranes," *J. Chem. Phys.*, **101**, 5274 (1994).

MacElroy, J. M. D., Seaton, N. A. and Friedman, S. F., "Sorption Rate Processes in Carbon Molecular Sieves," Ch. 17 in Equilibria and Dynamics of Gas Adsorption on Heterogeneous Solid Surfaces, W. Rudzinski, W. A. Steele and G. Zgrablich (Eds.), Elsevier, Amsterdam (1997).

MacElroy, J. M. D. and Suh, S.-H., "Single-File Counterdiffusion in Pores of Infinite and Finite Length," *Progress in Zeolite and Microporous Materials*, **105**, 1875 (1997a).

MacElroy, J. M. D. and Suh, S.-H., "Self-diffusion in Single-file Pores of Finite Length," *J. Chem. Phys.*, **106**, 8595 (1997b).

MacElroy, J. M. D., Seaton, N. A. and Friedman, S. P., "On the Origin of Transport Resistances within Carbon Molecular Sieves," *Chem. Eng. Sci.*, **54**, 1015 (1999).

MacElroy, J. M. D. and Boyle, M. J., "Nonequilibrium Molecular Dynamics Simulation of a Model Carbon Membrane Separation of CH_4/H_2 Mixtures," *Chem. Eng. J.*, **74**, 85 (1999).

Mason, E. A. and Malinauskas, A. P., "Gas Transport in Porous Media: The Dusty Gas Model," Elsevier, Amsterdam (1983).

Mason, E. A. and Viehland, L. A., "Statistical-mechanical Theory of Membrane Transport for Multicomponent Systems: Passive Transport through Open Membranes," *J. Chem. Phys.*, **68**, 3562 (1978).

Moore, S. V. and Trimm, D. L., "The Preparation of Carbon Molecular Sieves by Pore Blocking," *Carbon*, **15**, 177 (1977).

Mori, H., "Transport, Collective Motion, and Brownian Motion," *Prog. Theor. Phys.*, **33**, 423 (1965).

Nitta, T. and Furukawa, S., "Simulation Performance of a Non-Equilibrium Molecular Dynamics Method using Density Difference as a Driving Force," *Molec. Sim.*, in press (1999).

Pohl, P. I., Heffelfinger, G. S. and Smith, D. M., "Molecular Dynamics Simulation of Gas Permeation in Thin Silicalite Membranes," *Mol. Phys.*, **89**, 1725 (1996).

Pohl, P. I. and Heffelfinger, G. S., Massively Parallel Molecular Dynamics Simulation of Gas Permeation across Porous Silica Membranes," *J. Membrane Sci.*, **155**, 1 (1999).

Pozhar, L. A. and Gubbins, K. E., "Quasihydrodynamics of Nanofluid Mixtures," *Phys. Rev. E*, **56**, 1 (1997).

Pozhar, L. A. and Gubbins, K. E., "Transport Theory of Dense, Strongly Inhomogeneous Fluids," *J. Chem. Phys.*, **99**, 8970 (1993).

Rao, M. B. and Sircar, S., "Nanoporous Carbon Membranes for Separation of Gas Mixtures by Selective Surface Flow," *J. Membrane Sci.*, **85**, 253 (1993).

Ruthven, D. M., "Diffusion of Oxygen and Nitrogen in Carbon Molecular Sieve," *Chem. Eng. Sci.*, **47**, 4305 (1992).

Ruthven, D. M., Raghavan, N. S. and Hassan, M. M., "Adsorption and Diffusion of Nitrogen and Oxygen in a Carbon Molecular Sieve," *Chem. Eng. Sci.*, **41**, 1325 (1986).

Sahimi, M., "Applications of Percolation Theory," Taylor and Francis, London (1994).

Seaton N. A., Friedman, S. P., MacElroy, J. M. D. and Murphy, B. J., "The Molecular Sieving Mechanism in Carbon Molecular Sieves," *Langmuir*, **8**, 1199 (1997).

Suh, S. H. and MacElroy, J. M. D., "Molecular Dynamics Simulation of Hindered Diffusion in Microcapillaries," *Mol. Phys.*, **58**, 445 (1986).

Sunderrajan, S., Hall, C. K. and Freeman, B. D., "Estimation of Mutual Diffusion Coefficients in Polymer/Penetrant Systems using Nonequilibrium Molecular Dynamics Simulations," *J. Chem. Phys.*, **105**, 1621 (1996).

Thompson, A. P. and Heffelfinger, G. S., "Direct Molecular Simulation of Gradient-driven Diffusion of Large Molecules using Constant Pressure," *J. Chem. Phys.*, **110**, 10693 (1999).

Thompson, A. P., Ford, D. M. and Heffelfinger, G. S., "Direct Molecular Simulation of Gradient-driven Diffusion," *J. Chem. Phys.*, **109**, 6406 (1998).

Travis, K. P. and Gubbins, K. E., "Combined Diffusive and Viscous Transport of Methane in a Carbon Slit Pore," *Molec. Sim.*, in press (1999).

Tsapatsis, M. and Gavalas, G. R., "A Kinetic Model of Membrane Formation by CVD of SiO_2 and Al_2O_3," *AIChE J.*, **38**, 847 (1992).

Tsapatsis, M. and Gavalas, G. R., "Modelling of SiO_2 Deposition in Porous Vycor: Effects of Pore Network Connectivity," *AIChE J.*, **43**, 1849 (1997).

Tunca, C. and Ford, D. M., "A Transition-state Theory Approach to Adsorbate Dynamics at Arbitrary Loadings," *J. Chem. Phys.*, **111**, 2751 (1999).

Verlet, L., "Computer 'Experiments' on Classical Fluids. I. Thermodynamical Properties of Lennard-Jones Molecules," *Phys. Rev.*, **159**, 98 (1967).

Vertenstein, M. and Ronis, D., "Microscopic Theory of Membrane Transport. III. Transport in Multiple Barrier Systems," *J. Chem. Phys.*, **85**, 1628 (1986).

Voter, A. F., "A Method for Accelerating the Molecular Dynamics Simulation of Infrequent Events," *J. Chem. Phys.*, **106**, 4665 (1997).

Wicke, E. and Kallenbach, R., "The Surface Diffusion of Carbon Dioxide in Activated Charcoals," *Kolloid Z.*, **97**, 135 (1941).

Xu, L. F., Sedigh, M. G., Sahimi, M. and Tsotsis, T. T., "Nonequilibrium Molecular Dynamics Simulation of Transport of Gas Mixtures in Nanopores," *Phys. Rev. Lett.*, **80**, 3511 (1998).

Xu, L. F., Tsotsis, T. T. and Sahimi, M., "Nonequilibrium Molecular Dynamics Simulation of Transport and Separation of Gases in Carbon Nanopores. I. Basic Results," *J. Chem. Phys.*, **111**, 3252 (1999).

Zwanzig, R., "Memory Effects in Irreversible Thermodynamics," *Phys. Rev.*, **124**, 983 (1961).